Corrosion Study of Sn-9Zn Lead-Free Solder in Alkaline Solution

Muhammad Firdaus Mohd Nazeri, Muhammad Ghaddafy Affendy and Ahmad Azmin Mohamad[*]

School of Materials and Mineral Resources Engineering, Universiti Sains Malaysia, 14300, Nibong Tebal, Penang, Malaysia.
[*]E-mail: azmin@eng.usm.my

The corrosion potential and current of Sn-9Zn/Cu in 6 M KOH solution was investigated. The potential abruptly increases with increased immersion time before saturation at -1120 mV. The corrosion current drops significantly until it reaches a stable value at 10 µA. Morphological and elemental analyses reveal the formation of oxides on the surface after immersion. The post-immersion solder joint displays 22% reduction in ultimate tensile strength as a result of Sn and Zn consumption during the production of corrosion products at the bulk solder region of the Cu/Sn-9Zn/Cu butt joint.

1. INTRODUCTION

A solder is a part of an electronic packaging that plays various crucial roles, such as electrical and mechanical connections [1-3]. One of the most famous lead (Pb)-free solders is Sn-9Zn. A wide range of reliability issues involving tensile strength, creep resistance and melting point have been addressed to ensure that the new Pb-free solders can replace Sn-Pb in assembly and application without major modifications [4-7].

The corrosion behaviors of Pb-free solders have been extensively studied [8-15]. Lin et al. [9] have reported that Al-Zn-Sn solders produce very dense corrosion product layers of oxides, chlorides and oxychlorides that contribute to passivation behavior in sodium chloride (NaCl) solution. Rosalbino et al. [14, 15] agree that compact corrosion products can be obtained as corrosion byproducts of solders in 0.1 M NaCl. Li et al. [8] also reveals that Pb-free solders exhibit better corrosion resistance than Sn-Pb in 3.5 wt % NaCl.

Alkaline-based batteries that utilize 6 M potassium hydroxide (KOH) as the electrolyte are commonly used to supply electrical power to devices. However, any excessive loading or unexpected leakage from the batteries may wet the solders on the electronic circuit. The existence of copper (Cu) as bonding pad can also possibly induce galvanic corrosion with Sn-9Zn solder in the presence of KOH. Although known to be corrosive, studies on the corrosion properties of solders in KOH solution are very limited.

In the present study, the open circuit of potential and current of reflowed Sn-9Zn on Cu (Sn-9Zn/Cu) in 6 M KOH is studied. Morphological, elemental, phase and mechanical analyses are conducted to gain further understanding of the obtained potential and current behaviors.

2. EXPERIMENTAL

Sn and Zn were co-melted in the presence of nitrogen gas at 450 °C to produce Sn-9Zn solder alloy. Sn-9Zn plate was obtained by pressing the solidified solder with a hydraulic press, and punched to produce 5 mm-diameter solder pellets. The reflowing process of the Sn, Zn and Sn-9Zn solders on top of a 10×10 mm^2 Cu plate was performed at 250 °C for 10 s using a hotplate to produce Sn/Cu, Zn/Cu and Sn-9Zn/Cu. The sample was then cold-mounted with epoxy resin.

Sn/Cu, Zn/Cu and Sn-9Zn/Cu as the working electrodes versus Hg/HgO as the reference electrode were immersed in 6 M KOH for corrosion tests. Potential and current were recorded using a UT803 UNI-T multimeter equipped with data interface recording software. X-ray diffraction (XRD) was performed using a Bruker AXS D9 diffractometer to evaluate the structural changes. A field emission scanning electron microscopy (FESEM) system was used to characterize the morphological transformation. Alternatively, the elemental properties of the solder were studied by an energy dispersive X-ray (EDX) instrument coupled to a Zeiss Supra 35VP FESEM system.

For mechanical analysis, two Cu plates were used to create a Cu/Sn-9Zn/Cu butt joint with dimensions of $40.0 \times 5.0 \times 1.5$ mm^3. A hot plate was used in the soldering process. The temperature was maintained at 250 °C for 10 s with the application of ZnCl-based flux. The soldered joint was air cooled to solidify. Once cooled, the excess solder on the Cu plates were completely ground. The pull test was performed at a crosshead speed of 2 mm/min at room temperature to determine the tensile strength of the joint. Pre- and post-pull test images of the joint were taken by a Dinolite microscope to investigate the fracture surface further.

3. RESULTS AND DISCUSSION

3.1 Corrosion potential and current analyses

The corrosion potential behaviors of Sn/Cu, Zn/Cu, and Sn-9Zn/Cu after immersion in 6 M KOH are presented in Fig. 1. The control sample Sn/Cu shows a stable potential at -1050 mV, and Zn/Cu gives -1330 mV. On the contrary, Sn-9Zn/Cu undergoes two stages of potential change. Stage 1

demonstrates a sudden rise in corrosion potential from its initial potential point of -1330 to -1120 mV after 40 min. Stage 2 occurs after the completion of Stage 1. In Stage 2, the potential changes appear to be in a stable region, forming a long plateau of potential against time. The potential remains almost constant until the end of immersion.
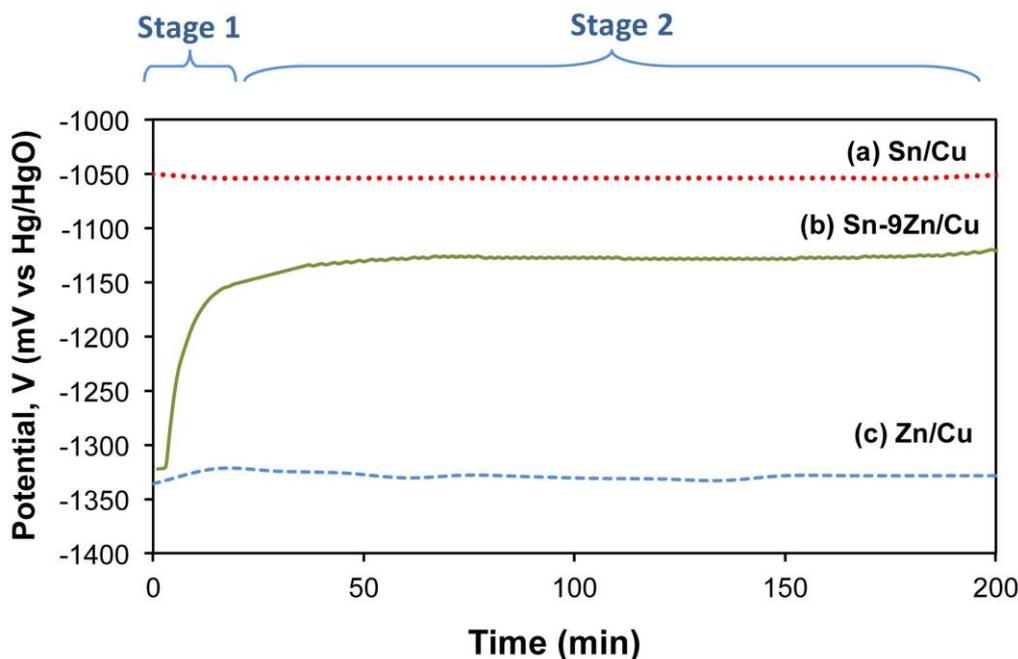
Figure 1. Corrosion potential plots of (a) Sn/Cu, (b) Sn-9Zn/Cu and (c) Zn/Cu against time in 6 M KOH.

The value of the initial potential obtained for Sn-9Zn/Cu at -1330 mV is almost the same as the open circuit potential of Zn/Cu in 6 M KOH. Zn is the first to be dissolved in 6 M KOH because it is more active than Sn and Cu. The specific reaction of Zn removal from Sn-9Zn/Cu at the early stage leads to dealloying or dezincification. The preferential dissolution process of specific elements in an alloy compound has also been observed by Alfantzi et al. [16]. This dissolution process contributes to the initiation of potential in Stage 1, according to the reaction [17]:

$$Zn \rightarrow Zn^{2+} + 2e^- \qquad (1)$$

There is a large amount of OH$^-$ ions in KOH electrolyte. As a result, the ions have higher ability to reach the solder alloy surface, contributing to the formation of ZnO [17]:

$$Zn^{2+} + 2\,OH^- \rightarrow Zn(OH)_2 \qquad (2)$$

$$Zn(OH)_2 \rightarrow ZnO + H_2O \qquad (3)$$

ZnO production and deposition causes Zn depletion and increased potential from -1330 mV to a much nobler value of -1120 mV. Once the solder surface is covered with ZnO, the contact between Zn and OH⁻ becomes difficult, leaving the potential to be saturated. Consequently, Stage 2 is allowed to start at a nobler potential value.

Given that Zn is the minor element in Sn-9Zn, Zn is quickly depleted or blocked by ZnO on the surface. Thus, Sn can be dissolved as the second most active material after Zn in this system. According to Alvarez et al. [18], Sn dissolves and passivates:

$$Sn + 2OH^- \rightarrow Sn(OH)_2 + 2e^- \qquad (4)$$

$$Sn(OH)_2 \rightarrow SnO + H_2O \qquad (5)$$
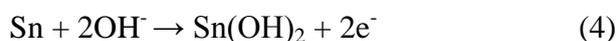
Subsequently, $Sn(OH)_4$ species form:

$$SnO + H_2O + 2OH^- \rightarrow Sn(OH)_4 + 2e^- \qquad (6)$$

$$Sn(OH)_2 + 2OH^- \rightarrow Sn(OH)_4 + 2e^- \qquad (7)$$
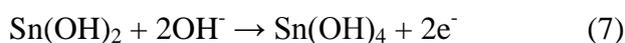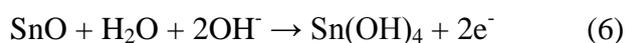
This species then dehydrates:

$$Sn(OH)_4 \rightarrow SnO_2 + 2H_2O \qquad (8)$$
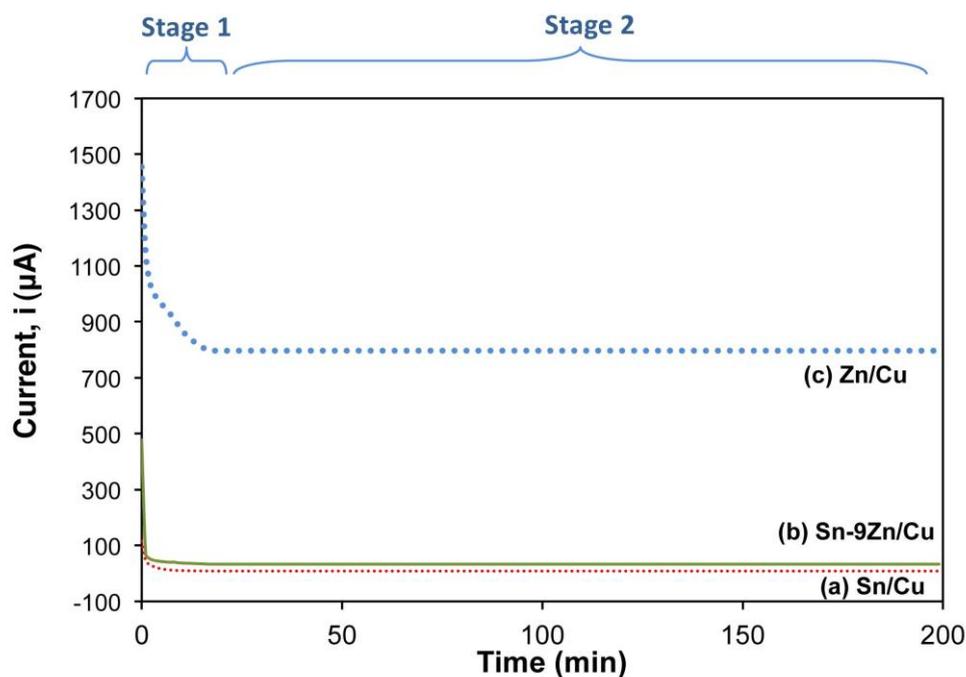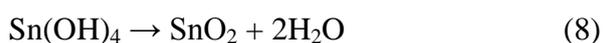
Figure 2. Corrosion current plots of (a) Sn/Cu, (b) Sn-9Zn/Cu and (c) Zn/Cu against time in 6 M KOH.

Fig. 2 shows the variations in the corrosion current (*i*) of Sn/Cu, Zn/Cu and Sn-9Zn/Cu in 6 M KOH solution. In general, all *i* profiles show sudden reductions immediately after immersion before forming steady plateaus. Zn gives the highest initial *i* at 1470 μA, which quickly drops to 1000 μA within only 5 min. This phenomenon is followed by a steady decrease for 20 min until reaching a stable *i* plateau at 800 μA. The starting current value for Sn-9Zn/Cu is 490 μA and *i* immediately plummets to ~10 μA. Within only 5 min, a steady plateau is formed and stabilized until the end of immersion. The *i* profile of Sn/Cu is strikingly similar to that of Sn-9Zn/Cu in 6 M KOH solution, except for a much lower initial *i* at 133.5 μA. The formation of a stable plateau of potential has also been achieved by other researchers [19, 20], who confirm that the formation of a surface corrosion product layer is attributed to Stage 2.

The fast reduction of *i* implies that Sn-9Zn alloy reverses its behavior upon contact with KOH. The passivation of alloys may contribute to this behavioral change. During the early stage of immersion, Sn-9Zn behaves anodically and Zn, as the most active material in the alloy, is the first to be oxidized. As a result of interaction with OH^- ions, the corrosion product ZnO is formed and deposited, thereby acting as a barrier for protecting Sn-9Zn from further reaction with OH^-. Accordingly, the surface of Sn-9Zn changes and becomes cathodic.

A large *i* signifies that the system undergoes high-magnitude corrosion [20, 21]. Zn/Cu gives the highest initial and stabilized *i* values in 6 M KOH solution. The position of the metal in the galvanic series plays a major contribution in corrosion. Zn/Cu is farther in this series compared with Sn-9Zn/Cu and Sn/Cu. Thus, a large value of *i* is produced because anode Zn is consumed rapidly in 6 M KOH. The small amount of Zn in Sn-9Zn allows Sn-9Zn/Cu to possess a slightly higher initial *i* than Sn/Cu. However, once Zn is depleted, *i* drops and the profile becomes identical with Sn/Cu.

3.2 Morphological, elemental and phase analyses

Fig. 3a shows the FESEM image of Sn-9Zn alloy before the corrosion analysis. The microstructure of Sn-9Zn is as expected from an alloy of eutectic composition. The fine eutectic lamellar structure is found in the form of dark needle-like Zn-rich phases distributed in the matrix of Sn. After immersion in 6 M KOH (Fig. 3b), the surface roughens. The deposition of corrosion products as a compound is believed to be the reason for this characteristic. This rough layer covers the entire surface. However, there are significant cracks on this layer.

EDX analysis was performed on the Sn-9Zn solder surface before and after immersion in 6 M KOH. Sn has the dominant percentage (91 wt %) in Sn-9Zn before immersion in the scanned area (Fig. 3a). After immersion (Fig. 3b), three elements, Sn, O and Zn, are detected. Sn still dominates the composition at 63 wt %, followed by O as the new element (22 wt %) and finally Zn (14 wt %). The detection of O forming the corrosion product compound with Sn and Zn confirms that OH^- reacts with the oxidized Sn and Zn during immersion in 6 M KOH. The corrosion products can either be SnO, SnO_2, ZnO or the combinations of all these oxides. There are observed cracks linked with one another

on the surface of the rough corrosion product layer, suggesting that the layer formed is brittle and mechanically weak.
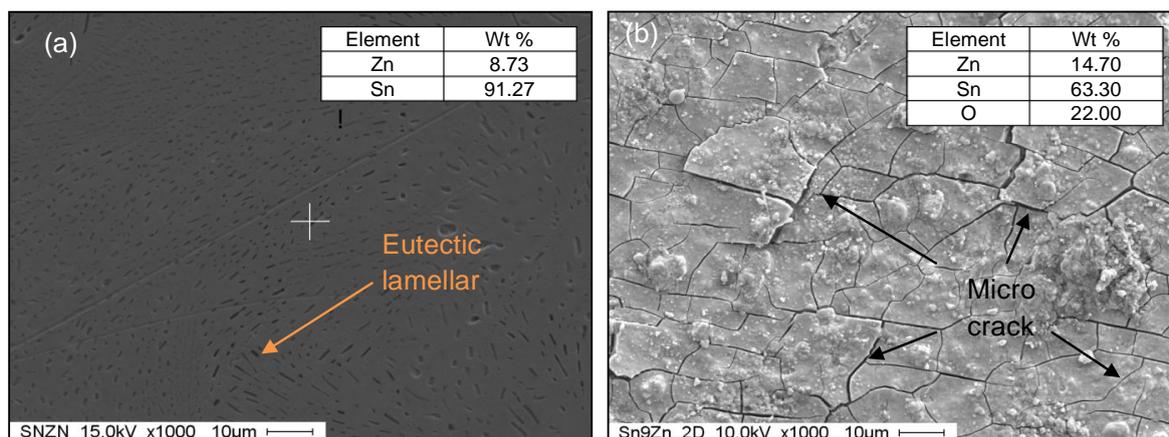
Figure 3. Microscopy and elemental analyses of Sn-9Zn (a) before and (b) after immersion in 6 M KOH.
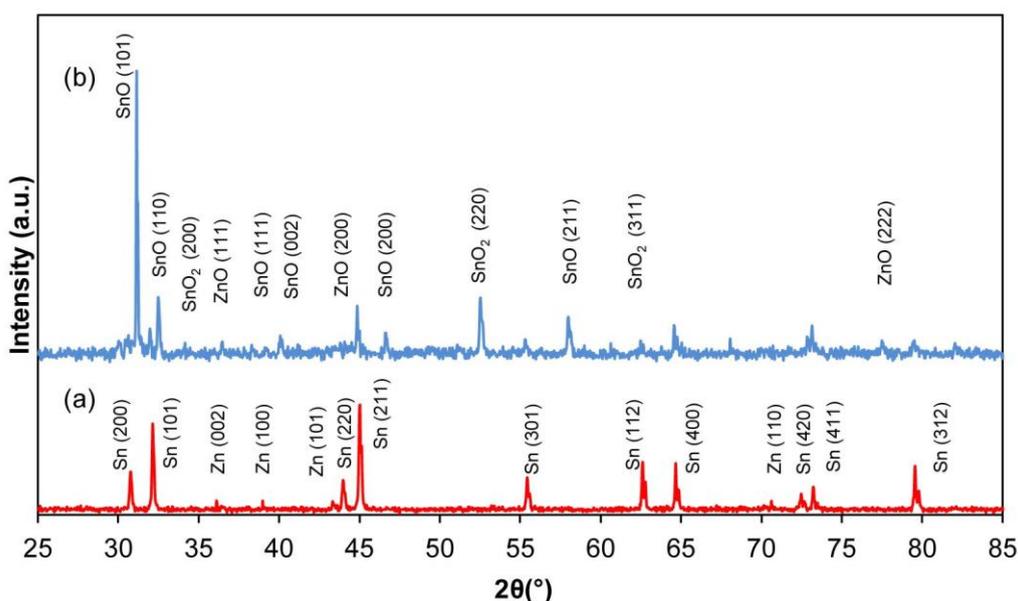
Figure 4. XRD patterns of Sn-9Zn (a) before and (b) after immersion in 6 M KOH.

Fig. 4 shows the XRD pattern of Sn-9Zn before and after immersion in 6 M KOH. Two phases are detected for Sn-9Zn solder before immersion, namely, those of Sn and Zn. This result is in accordance with that obtained from EDX analysis. Sn is matched with ICDD file no. 03-065-2631, whereas 01-087-0713 is for Zn. There are 10 different peaks of Sn observed, with Sn (211) as the most dominant at $2\theta = 44.91°$. On the other hand, only four peaks of Zn are found. Significant changes in the phases are observed after immersing Sn-9Zn in 6 M KOH. Three new phases of tin oxides, namely, SnO (ICDD 00-024-1342) and SnO_2 (ICDD 00-033-1374), are recorded. In contrast, the only zinc

oxide is ZnO (ICDD 03-065-0682). Among the three new phases, SnO is the major oxide as evidenced by six different peaks and shows the highest intensity at 30.80° (101).

The original peaks of Sn and Zn are either decreased or diminished after coming into contact with 6 M KOH. The loss of intensities highlights that both original phases are either consumed to produce the new oxide phases as corrosion products or undetected as a result of being covered by the deposited rough corrosion product layer. Thus, the results of the corrosion potential and current analyses, as well as microstructural analysis are further validated.

3.3 Mechanical property analysis

The effect of KOH solution on the mechanical properties of Cu/Sn-9Zn/Cu butt joint is shown in Fig. 5. The stress obviously increases linearly with increased load.
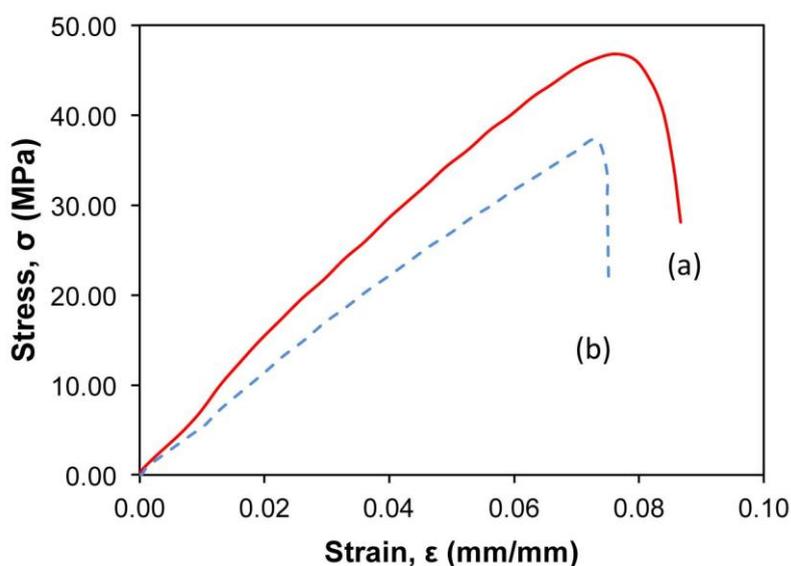
Figure 5. Stress-strain curves of Cu/Sn-9Zn/Cu butt joint (a) before and (b) after immersion in 6 M KOH.

The ultimate tensile strength (UTS) of the as-prepared joint is 45 MPa and peaks at a strain value of 0.075. However, after immersion, the Cu/Sn-9Zn/Cu butt joint undergoes reduction in both UTS and strain. The UTS is reduced by 22% to 35 MPa after immersion. On the other hand, the strain at the UTS changes to 0.074. The stress-strain curves also reveal that the tensile stress value sharply drops after the peak compared with the as-prepared joint. This result indicates the lack of ductility of the joint after immersion.

Fig. 6 shows the macrostructural images of as-prepared Cu/Sn-9Zn/Cu butt joint after immersion in 6 M KOH and after failure under tensile loading. The as-prepared joint (Fig. 6a) reveals that the Cu plates are well attached to the shiny, grayish Sn-9Zn solder. After immersion (Fig. 6b), the solder are significantly darkened, enabling the boundaries between the Cu plates and Sn-9Zn to

become clearer. The solder region also appears to be dull and has lost its original appearance before immersion. The post-tensile analysis image is shown in Fig. 6c. The joint failure is due to the formation of crack through the solder region, implying that the interfaces of the joint are well connected. Small necking regions can be observed along the crack.
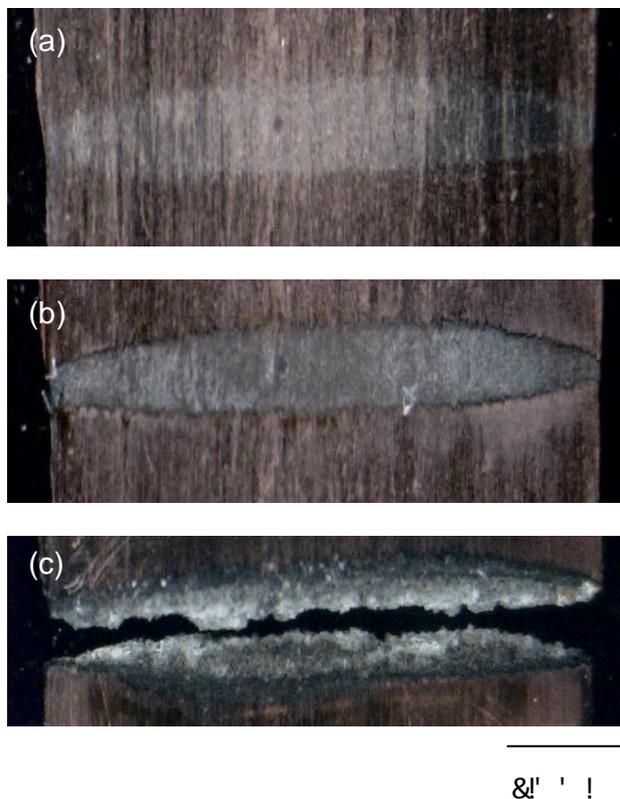
Figure 6. Macroscopic images of Cu/Sn-9Zn/Cu butt joint (a) before immersion in 6 M KOH, (b) after immersion in 6 M KOH and (c) after tensile test.
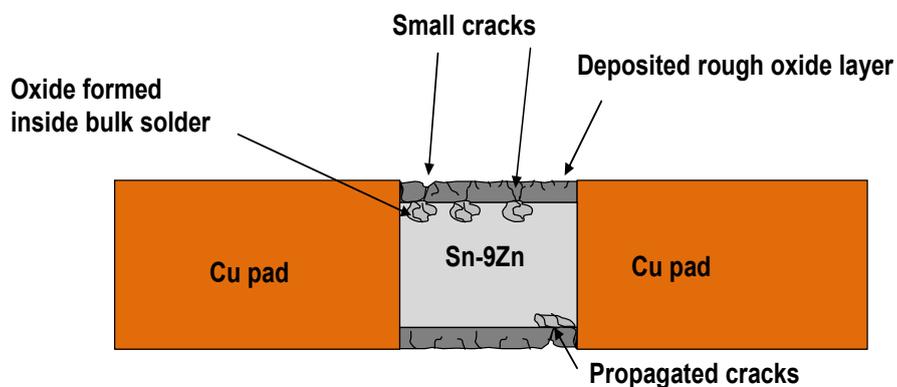
Figure 7. Schematic diagram of Cu/Sn-9Zn/Cu butt joint after immersion in 6 M KOH (side view).

Fig. 7 shows the schematic cross-section of Cu/Sn-9Zn/Cu butt joint after immersion in 6 M KOH. Sn and Zn from the bulk solder region are consumed to produce SnO, SnO_2 and ZnO, leading to the formation of small cracks. The oxides produced are co-deposited and forms a rough oxide layer on the solder surface. With the brittle nature of oxides replacing Sn and Zn, the mechanical integrity of the joint is weakened. The existence of linked cracks throughout the surface also allows further penetration of OH^- into the rough oxide layer, causing the cracks to propagate deeper in the bulk solder region and produce more undesirable brittle oxides. Accordingly, the strength of the joint is directly affected, causing UTS loss and sharply decreased tensile stress after UTS is achieved as load applied to the joint.

4. CONCLUSIONS

The corrosion potential and current of Sn-9Zn changes in two stages with increased immersion time in 6 M KOH. Complex oxides develop on the solder surface to stutter the dissolution of active materials in the first stage. The formation of the corrosion product layer consequently produces the stable second stage. The stress-strain curve shows UTS loss after immersing the Cu/Sn-9Zn/Cu butt joint in 6 M KOH. This result shows that the reliability of the Sn-9Zn solder joint is significantly affected when in contact with KOH electrolyte in real-life applications. The formation of linked cracks as revealed by FESEM makes the oxides more brittle, allowing further penetration of OH^- on the solder surface and consequently weakening the joint strength.

References

1. M. Abtew, G. Selvaduray, *Mater. Sci. Eng. R-Rep.*, 27 (2000) 95-141.
2. Q.V. Bui, N.D. Nam, B.I. Noh, A. Kar, J.G. Kim, S.B. Jung, *Mater. Corros.*, 61 (2010) 30-33.
3. R.K. Shiue, L.W. Tsay, C.L. Lin, J.L. Ou, *Microelectron. Reliab.*, 43 (2003) 453-463.
4. T.-C. Chang, S.-M. Chou, M.-H. Hon, M.-C. Wang, *Mater. Sci. Eng. A- Struct. Mater. Prop. Microstruct. Process*, 429 (2006) 36-42.
5. T.-C. Chang, M.-H. Hon, M.-C. Wang, *J. Electron. Mater.*, 32 (2003) 516-522.
6. T.-C. Chang, J.-W. Wang, M.-C. Wang, M.-H. Hon, *J. Alloy. Compd.*, 422 (2006) 239-243.
7. M.N. Islam, Y.C. Chan, M.J. Rizvi, W. Jillek, *J. Alloy. Compd.*, 400 (2005) 136-144.
8. D. Li, P.P. Conway, C. Liu, *Corrosion Sci.*, 50 (2008) 995-1004.
9. K.-L. Lin, T.-P. Liu, *Mater. Chem. Phys.*, 56 (1998) 171-176.
10. U.S. Mohanty, K.-L. Lin, *Mater. Sci. Eng. A- Struct. Mater. Prop. Microstruct. Process*, 406 (2005) 34-42.
11. U.S. Mohanty, K.-L. Lin, *Corrosion Sci.*, 48 (2006) 662-678.
12. U.S. Mohanty, K.-L. Lin, *Appl. Surf. Sci.*, 252 (2006) 5907-5916.
13. U.S. Mohanty, K.-L. Lin, *Corrosion Sci.,* 50 (2008) 2437-2443.

14. F. Rosalbino, E. Angelini, G. Zanicchi, R. Carlini, R. Marazza, *Electrochim. Acta*, 54 (2009) 7231-7235.
15. F. Rosalbino, E. Angelini, G. Zanicchi, R. Marazza, *Mater. Chem. Phys.*, 109 (2008) 386-391.
16. A.M. Alfantazi, T.M. Ahmed, D. Tromans, *Mater. Des.*, 30 (2009) 2425-2430.
17. A.A. Mohamad, *J. Power Sources*, 159 (2006) 752-757.
18. P.E. Alvarez, S.B. Ribotta, M.E. Folquer, C.A. Gervasi, J.R. Vilche, *Corrosion Sci.,* 44 (2002) 49-65.
19. D. Mercier, M.G. Barthes-Labrousse, *Corrosion Sci.,* 51 (2009) 339-348.
20. N.A. Popovich, R. Govind, *J. Power Sources*, 112 (2002) 36-40.
21. N.M. Taher, A.S. Al Jabab, *Dent. Mater.,* 19 (2003) 54-59.
22. W. Xue, C. Wang, H. Tian, Y. Lai, *Surf. Coat. Technol*., 201 (2007) 8695-8701.